Free Energy Simulations of Active-Site Mutants of Dihydrofolate Reductase

ARTICLE *in* THE JOURNAL OF PHYSICAL CHEMISTRY B · NOVEMBER 2014

Impact Factor: 3.3 · DOI: 10.1021/jp5059963 · Source: PubMed

THE JOURNAL OF PHYSICAL CHEMISTRY B

Article

pubs.acs.org/JPCB

Free Energy Simulations of Active-Site Mutants of Dihydrofolate Reductase

Dvir Doron,[†] Vanja Stojković,[‡,§,#] Lokesh Gakhar,[§] Alexandra Vardi-Kilshtain,[†] Amnon Kohen,[‡] and Dan Thomas Major*[,†]

[†]Department of Chemistry and the Lise Meitner-Minerva Center of Computational Quantum Chemistry, Bar-Ilan University, Ramat-Gan 5290002, Israel

[‡]Department of Chemistry, University of Iowa, Iowa City, Iowa 52242, United States

[§]Protein Crystallography Facility and Department of Biochemistry, University of Iowa, Iowa City, Iowa 52242, United States

Supporting Information

ABSTRACT: This study employs hybrid quantum mechanics−molecular mechanics (QM/MM) simulations to investigate the effect of mutations of the active-site residue I14 of *E. coli* dihydrofolate reductase (DHFR) on the hydride transfer. Recent kinetic measurements of the I14X mutants (X = V, A, and G) indicated slower hydride transfer rates and increasingly temperature-dependent kinetic isotope effects (KIEs) with systematic reduction of the I14 side chain. The QM/MM simulations show that when the original isoleucine residue is substituted in silico by valine, alanine, or glycine (I14V, I14A, and I14G DHFR, respectively), the free energy barrier height of the hydride transfer reaction increases relative to the wild-type enzyme. These trends are in line with the single-turnover rate measurements reported for these systems. In addition, extended dynamics simulations of the reactive Michaelis complex reveal enhanced flexibility in the mutants, and in particular for the I14G mutant, including considerable fluctuations of the donor−acceptor distance (DAD) and the active-site hydrogen bonding network compared with those detected in the native enzyme. These observations suggest that the perturbations induced by the mutations partly impair the active-site environment in the reactant state. On the other hand, the average DADs at the transition state of all DHFR variants are similar. Crystal structures of I14 mutants (V, A, and G) confirmed the trend of increased flexibility of the M20 and other loops.

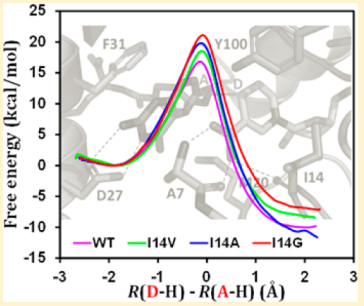

1. INTRODUCTION

Dihydrofolate reductase (DHFR; EC 1.5.1.3) is a ubiquitous enzyme catalyzing the reduction of dihydrofolate (DHF or H_2folate) by nicotinamide adenine dinucleotide phosphate hydride (NADPH) to form tetrahydrofolate (THF or H_4folate) and $NADP^+$. Its principal function is to maintain intracellular pools of THF, a compound essential for the biosynthesis of purines, thymine nucleotides, and several amino acids. Due to its pivotal role in nucleotide biosynthesis in many organisms, DHFR has long been recognized as an important target for various therapeutic purposes, in particular anticancer and antibacterial drugs, such as methotrexate (MTX) and trimethoprim, respectively.[1,2] The clinical importance of DHFR, along with its relatively modest size, has led many researchers to study, both experimentally and theoretically, the catalytic mechanism and kinetics of the DHFR redox reaction.

The key chemical step is a stereospecific transfer of the *pro-R* hydrogen at the C4 position of the nicotinamide ring in NADPH to the *re* face of the C6 atom of the pterin ring in DHF, with concomitant protonation at N5 (Scheme 1 and Figure 1).[3,4] The X-ray structure of the ternary complex of *Escherichia coli* DHFR (*ec*DHFR) crystallized with folate and the oxidized cofactor (i.e., E:folate:$NADP^+$)[5] is considered to reliably mimic the reactive configuration of the Michaelis

Scheme 1

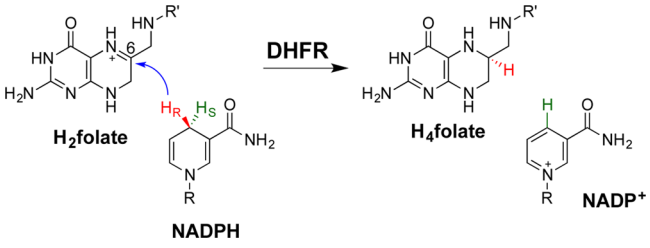

complex of the enzyme. In this conformation, a flexible segment of ca. 15 amino acid residues within the major domain, termed the M20 loop, packs against the nicotinamide ring of the cofactor, closing over the active site. This closed conformation might be associated with the C−H → C transfer (i.e., the M20 loop deletion mutant is still active, although it is much slower).[6]

The interactions exerted by active site residues proximal to the donor−acceptor moieties are likely to play a role in

Special Issue: William L. Jorgensen Festschrift

Received: June 17, 2014
Revised: November 5, 2014
Published: November 8, 2014

   dx.doi.org/10.1021/jp5059963 | *J. Phys. Chem. B* 2015, 119, 906−916

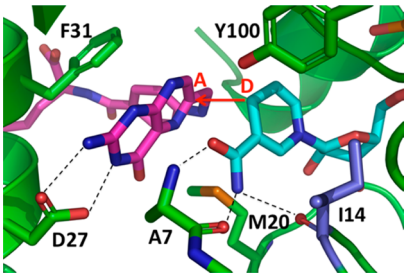

Figure 1. Portion of the protein structure and the bound ligands in the Michaelis complex of *E. coli* DHFR, based on X-ray data for the ternary complex E:folate:$NADP^+$ (PDB ID 1RX2). The active site is shown with the main species addressed in this work: the substrate (folate, magenta), the cofactor $NADP^+$ (blue); and three amino acid residues, including I14, A7 (both hydrogen bonded to the proximal carboxamide group of the nicotinamide moiety), and D27 and Y100, the only ionizable active site residues, hydrogen bonded to the pterin ring in folate. The donor and the acceptor carbons are denoted by a red arrow from donor to acceptor.

modulating the relative orientation of the reacting fragments as they approach one another along the hydride transfer reaction pathway. In that sense, the donor−acceptor distance (DAD) is a useful, chemically intuitive variable to follow. Thus, it is desirable to examine the contribution of the enzyme environment by scrutinizing the influence of direct structural perturbations of the reacting fragments and the DAD, and especially the relation between these and the free energy profile of the reaction. In this regard, recent studies of transition path sampling (TPS) simulations by Schwartz and co-workers have shown that unlike other enzymes (such as human lactate dehydrogenase[7]) in which nonequilibrated, fast (subpicosecond) dynamics was suggested to be coupled to the reaction coordinate, the protein motions in DHFR are presumably not directly coupled to the compressive promoting vibration along the DAD axis as the enzymatic reaction crosses the transition state.[8] Other computational studies have addressed the question of correlation between ns-ps motions and the reaction coordinate, as well as effects of mutations on the DAD fluctuations on both ground state (GS) and transition state (TS).[9−19]

Recently, we measured the single turnover rates at 25 °C and extracted the intrinsic kinetic isotope effect (KIE) over a temperature range of 5−45 °C for a series of active-site mutants of *ec*DHFR, in which the size of the side chain of residue 14 was systematically decreased from Ile in the wild-type (WT) enzyme to Val, Ala and Gly.[20,21] In this approach, the experiments yielded a controlled change with minimal alteration of the active-site electrostatics, while focusing on the changes to the carbon DAD. It was found that a smaller side chain behind the nicotinamide ring resulted in slower hydride transfer rates and increased temperature dependency of the intrinsic KIEs. In addition, molecular mechanics (MM) molecular dynamics (MD) simulations at room temperature for the enzyme ground state (GS, i.e. the Michaelis complex) were performed. These simulations suggested that the WT enzyme had an exclusive population characterized by narrow distributions of short GS DADs and angle between the planes of the nicotinamide and pterin rings, around the average values (3.58 Å and 29°, respectively). As expected, the mutants deviated significantly from these ideal values, with larger average DADs and a concomitant reduction in the population of the presumed reactive conformer with similar DADs to WT DHFR. Although not necessarily related, both lower rates and steeper temperature dependence of the intrinsic KIEs were correlated with the longer GS DADs and broader distributions of the GS DADs. Within the framework of a Marcus-like model, the temperature dependence of the KIEs only reflects the distribution of DADs at the TS (tunneling ready state, or QM delocalized TS) but is not affected by the GS DADs. Taken together, the hydrophobic side chain of I14 assists the hydride transfer by both, restricting the distribution and dynamics of the GS DAD and that of the DAD distribution at the TS.

In this work, we seek to complement the experiments performed in ref 21 from a theoretical vantage point by conducting extensive hybrid quantum mechanics (QM) and classical mechanics (CM) simulations of the hydride transfer reaction in *ec*DHFR. The free energy profiles were obtained for the WT *ec*DHFR and the aforementioned mutations of residue 14. Our approach takes advantage of the hybrid QM(AM1-SRP)/MM methodology employed in our earlier studies of DHFR[22−26] and formate dehydrogenase[27] systems, which has been shown to yield an accurate potential energy surface of the modeled reaction, as well as the integrated path integral (PI) and umbrella sampling (US) method.[28−32] This paper demonstrates the ability of state-of-the-art computational techniques to discriminate between mutations that alter the active site in a serial fashion (e.g., WT vs I14 active-site mutants). As a final introductory note, we stress that the current work integrates many of the important contributions of Jorgensen and co-workers to the field of molecular simulations: all-atom force-fields, the TIPnP water models and free energy methods, and the interfacing between force-fields and QM methods.[33−35]

2. METHODS

Construction of Mutant Enzymes. The initial coordinates of the mutant enzymes were constructed in silico by changing the Ala residue, I14, in the original WT *ec*DHFR structure (used in our introductory study[22]) to Val, Ala, or Gly. The setup and the MD simulations of all systems were carried out on the basis of procedures similar to those employed for the WT DHFR.[22−24] Briefly, the protonation states of all polar amino acid residue side chains were adjusted to pH 7, and the protonation states of the His residues (either the neutral tautomeric forms or the positively charged form) were determined so as to match the hydrogen bonding patterns in the nearest environment. The N5 position on the pterin ring of the substrate (dihydrofolate) was protonated. The HBUILD facility in the program CHARMM was applied to add hydrogen atoms. Fourteen sodium ions were added to the four isocharged WT and mutant systems to neutralize the overall negative charge.

Potential Energy Surface. The potential energy surface in the current study is described by a hybrid QM/MM Hamiltonian,[36] where the QM region is treated by a modified AM1[37] semiempirical Hamiltonian, denoted AM1-SRP (specific reaction parameters).[38] This Hamiltonian has been designed to reproduce high-level calculations for an assortment of electronic and thermodynamic properties for reactions involving various nicotinamide and pterin derivatives.[22] The QM region includes fragments of DHF and NADPH, which are proximal to the reaction center, whereas the MM region contains the remaining ligand atoms, the entire protein, water molecules, and sodium ions. The water molecules were represented by the three-point charge TIP3P model.[33]

dx.doi.org/10.1021/jp5059963 | J. Phys. Chem. B 2015, 119, 906−916

Hydrogen link atoms were placed across the bonds intersected by the QM/MM boundary, and the QM/MM interactions were treated by electrostatic embedding. A detailed QM/MM partitioning scheme and a thorough description of the development of the AM1-SRP Hamiltonian is provided elsewhere.[22] In modeling the MM region, we used the all-atom CHARMM36[39−42] force field, which has been reoptimized on the basis of studies of protein folding, assembly, and functionally relevant conformational changes. Such force-field fine-tuning was recently shown to be essential in order to correctly treat proteins in micro- and millisecond simulations.[43]

Molecular Dynamics Simulations. Periodic boundary conditions were employed to solvate the Michaelis complex using a pre-equilibrated cubic water box (∼65 Å × ∼65 Å × ∼65 Å), while treating long-range electrostatic interactions with the Ewald summation technique (64 × 64 × 64 FFT grid, κ = 0.340 Å^{-1}).[44] All systems were fully minimized, heated up gradually to 298 K for 25 ps, and equilibrated at that temperature for 1 ns at the MM level of theory. Each system was thereafter re-equilibrated using the QM(AM1-SRP)/MM potential over the course of 200 ps. All equilibrations were conducted with the isothermal−isobaric (NPT) ensemble at 1 atm and the target temperature was controlled by the extended constant pressure/temperature (CPT) method[45] and the Hoover thermostat.[46] The leapfrog integration scheme[47] was used to propagate the equations of motions, and the SHAKE algorithm[48] was applied to constrain all MM bonds involving hydrogen atoms, allowing a time step of 1 fs. During the equilibration, several nuclear Overhauser effect (NOE) restraints were imposed on key hydrogen bond interactions between the ligands and the surrounding residues, and removed 100 ps before moving on to the production phase. All enzyme simulations used a development version of the CHARMM program.[49,50] Complementary details of the MD simulations are available in our earlier work.

Potential of Mean Force. The US technique[51] was used to determine the classical-mechanical potential of mean force (CM-PMF) for the hydride transfer reaction at five target temperatures (5, 15, 25, 35, 45 °C). The reaction coordinate was defined as the antisymmetric reactive stretch coordinate, ζ_{asym}, namely, the difference between the lengths of the breaking C4−H and forming H−C6 bonds. A total of 17 individual US MD simulations ("windows") were performed along discrete, evenly spaced values of ζ_{asym} from −2.0 to 2.0 Å. Each window was subject to an appropriate harmonic restraint, which keeps ζ_{asym} in the desired region, and an umbrella potential (roughly the negative of the PMF) as a function of ζ_{asym}. In order to efficiently update the biasing potential as necessary, each window was sampled in multiple successive series with a predetermined number of MD steps. A typical simulation starts with a short equilibration (2 ps), followed by collection of the probability densities of configurations (ρ) along the reaction coordinate, ζ_{asym}. Whenever the biasing potential is updated, the subsequent simulation commences with a short equilibration, and the accompanying equilibration data is discarded. The cumulative simulation time per window was 275−375 ps. The statistics for the reaction coordinate was sorted into bins of width 0.01 Å. The positions and velocities of the last recorded configuration in a specific window were used to start its successor, to maintain continuity of propagation. In particular, the phase space variables reached at the end of the most current simulations at 25 °C were also the starting points for the simulations at both 15 and 35 °C. Similarly, simulations at 5 and 45 °C were each initiated from the respective end points determined in the simulations at the "neighboring" temperatures, 15 and 35 °C. CM-PMF curves and surfaces were computed using a multidimensional version of the weighted histogram analysis method (WHAM).[52]

QM PMFs were obtained by PI-US simulations as described in our earlier work.[22]

Materials and Methods. The mutants were expressed, purified, and stored as reported for other DHFR mutants.[53] Prior to preparation of ternary complexes for crystallization, purified proteins were loaded onto a Superdex-75 (GE) gel filtration column pre-equilibrated with the buffer containing 20 mM Tris-HCl, pH 7.5. DHFR eluted in a single peak, which was tested for monodispersity using dynamic light scattering on a NanoStar instrument (Wyatt Technology). Concentration of the pooled fractions was measured using UV absorbance at 280 nm and Bradford assay. Due to its low solubility, folate was added to a dilute protein solution at 10-fold molar excess relative to the concentration of the DHFR variant. The sample was incubated on ice for at least 1 h, after which it was filtered using Milipore 0.22 μm filter. The binary complex was then concentrated to a final concentration of ∼15 mg/mL (as determined by a Bradford assay). $NADP^+$ was added as a solid to the concentrated binary DHFR-Folate complex at 5-fold molar excess of DHFR.

All enzyme-Folate-$NADP^+$ ternary complexes were crystallized via the hanging drop vapor diffusion method by mixing 400 nl crystallization solution and 400 nl of prepared ternary complex using TTP LabTech Mosquito, except I14G DHFR where crystals were obtained through macroseeding into 4 μL drops (2 μL crystallization solution and 2 μL of protein complex).

To describe in greater detail, I14G-$NADP^+$-Folate crystallized in the $P2_12_12$ space group after macroseeding under the following conditions: 16 mg/mL I14G DHFR, 0.1 M Tris, pH 8.5, 0.9 M LiCl, and 36% w/v PEG 6,000; at 18 °C. Crystals appeared within 7 days after macroseeding.

I14V-$NADP^+$-Folate ternary complex crystallized in the $P2_1$ space group under the following conditions: 16 mg/mL I14V DHFR, 0.1 M Tris, pH 8.5, 0.1 M LiCl, and 34.2% w/v PEG 6,000; at 18 °C, within 2 weeks.

I14A-$NADP^+$-Folate ternary complex was crystallized in $P2_1$ space group under the following conditions: 15 mg/mL I14A DHFR, 0.2 M Lithium acetate, and 20% w/v PEG 3,350; at 18 °C, within 7 days.

Data Collection and Structure Determination. Crystals were flashed-cooled in liquid nitrogen, and data were collected at 100 K at the 4.2.2 synchotron beamline at the Advance Light Source of the Lawrence Berkley National Laboratory. The data were processed using either XDS[54] (for the I14A and I14G mutants), or d*TREK (for the I14V mutant).[55] The structures were solved by molecular replacement in PHASER,[56] part of the CCP4 suite,[57] using the structure of WT *ec*DHFR (PDB 1RX2) with the ligands removed to generate an initial model. Refinement and model building for all structures were done using REFMAC[58] and COOT.[59] All structures were refined with good geometry (RMS deviations in bond lengths were 0.013−0.03 Å, RMS deviation in bond angles were 1.72−2.54°), with the possible exception of the I14A structure, which showed higher overall temperature factor for molecule B. These problems are probably a result of static disorder. Data processing and final refinement statistics are given in Table S4.

dx.doi.org/10.1021/jp5059963 | J. Phys. Chem. B 2015, 119, 906−916

3. RESULTS

Free Energy Profiles. We obtained the CM-PMFs for the catalyzed transfer of hydride from NADPH to DHF in the wild-type DHFR (WT DHFR) and three I14 mutants, namely I14V, I14A, and I14G DHFR (Figure 1), at 5, 15, 25, 35, and 45 °C. Figure 2 shows the CM-PMFs for WT DHFR and the active-site mutants at 25 °C. The CM-PMFs at 5, 15, 25, 35, and 45 °C are provided as Supporting Information (Figure S1 and Table S1). Examination of the CM-PMFs at 25 °C provides some important findings. The free energy of activation for the WT enzyme, $\Delta G^{\ddagger}$, is 16.8 kcal/mol, while the reaction free energy, ΔG_r, is −9.7 kcal/mol. The presence of a slightly less bulky side chain in the I14V DHFR system causes a slight increase in the free energy barrier (18.5 kcal/mol) relative to WT DHFR. Further truncation of the side chain brings about even higher free energy barriers, as evident by the $\Delta G^{\ddagger}$ value for the I14A and I14G systems (19.8 and 21.1 kcal/mol, respectively), indicative of a progressive reduction in rate as the mutation becomes more substantial. This general trend is in accordance with our experimental work in refs 20−21, which found a correlation between reduced side chain volume and diminished single-turnover rates of the hydride transfer. At the same time, the reaction becomes less exothermic as the free energy barrier increases in the series in the WT−I14V-I14G, indicating a diminished driving force for the hydride transfer caused by the mutation. These trends are reminiscent of recent QM/MM studies of the remote mutations G121 V, M42W, and G121 V-M42W in *ec*DHFR, conducted by us[25] and others.[17] An exception to the above said trend is I14A DHFR, whose estimated free energy of reaction is comparable to that of the native enzyme. Interestingly, the temperature seemingly has little effect on the computed CM-PMF (Figure S1 and Table S1).

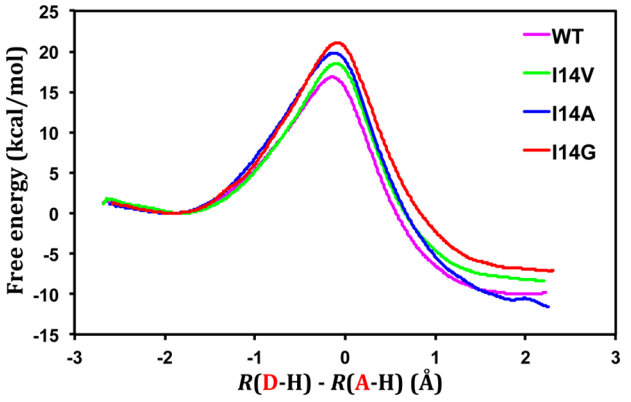

Figure 2. Classical mechanical potentials of mean force for the hydride transfer in WT DHFR and Ile14 mutants, computed at 25 °C. The antisymmetric stretch coordinate, ζ_{asym}, is defined as the difference in the distance of the transferring hydrogen from the donor carbon of the cofactor and the acceptor carbon of the substrate.

The quantum corrected $\Delta G^{\ddagger}$'s obtained from combined classical free energy and quantum PI simulations are compared with the values obtained from the single-turnover rates of ref 21 and the Eyring equation. To assess the quality of the results, we compare them to kinetic measurements for the WT DHFR[53,60−62] and the I14 mutants,[21] all of which were conducted using a similar experimental protocol under the same conditions (pH 7). Notably, the presteady-state single-turnover rates at pH 7 are not representative of the C−H → C transfer step *per se*, as it is still somewhat masked by nonchemical steps such as ligand binding and conformational rearrangements (i.e., kinetic complexity), as evident from a smaller observed KIE relative to its intrinsic value.[63] Moreover, available data from different kinetic studies of WT *ec*DHFR show a linear increase of the activation barrier with pH for the single turnover measurements (13.4,[64] 14.2−14.3,[53,60,61,65] 16.7[66]-16.9,[62] and 17.5[65] kcal/mol at pH 6.5, 7, 9, and 9.5, respectively)—further indicating that the single-turnover rate measurements must include the N5-DHF protonation step, which precedes the hydride transfer step calculated here. In our models, the titratable/ionizable residues in both the native and mutated proteins were constructed considering a neutral pH environment. As can be inferred from Table S1, inclusion of NQEs lowered the free energy barrier from classical MD simulations by 2.0−2.4 kcal/mol, which is similar to our earlier work,[22] that estimated by Hammes-Schiffer and co-workers (2.4 kcal/mol),[9] where the transferring hydrogen nucleus was represented as a three-dimensional wave function, and lower by ∼1 kcal/mol than that predicted by Gao and co-workers using either ensemble-averaged variational transition state theory with multidimensional tunneling (EA-VTST/MT)[67,68] or the PI-UM[17] approaches. Overall, the calculated free energy barriers are in good agreement with the experimental ones, and basically conform to the general trend due to the I14 mutations.

Impact of Mutation on Structure. From a structural standpoint, the varying magnitudes of the experimentally derived free energy barriers in the WT enzyme and the I14 mutants may reflect differences in the relative probabilities of sampling conformations that are conducive to the hydride transfer process. These conformations are directed toward generating reactant and transition state configurations with favorable geometry of the reactants and optimized stabilizing interactions within the active-site environment.[13] In this work, the starting structures of all three mutants were created by point mutation based on the coordinates of the ternary complex of WT DHFR with folate and $NADP^+$ (PDB ID: 1RX2),[5] crystallized in the $P2_12_12_1$ space group, in which the M20 loop adopts the closed conformation. The basic premise in our simulation approach was that the mutant enzymes adopt a structure similar to that of the WT enzyme, and that MD propagation allows the mutants to relax into their correct Boltzmann distribution. The analogous ternary complexes for all three mutations of I14 in *ec*DHFR were crystallized and their structures determined. In particular, the I14A and I14V structures were only obtained in the $P2_1$ space group, where the M20 loop is always observed in the open conformation (i.e., also in WT) as the open conformation is seemingly stabilized by crystal contacts. It is plausible that a transient population of the open conformational state may play a role in the catalytic cycle since: (i) the open conformation facilitates both substrate binding and product release; and (ii) replacement of the part of the M20 loop (residues 16−19) with glycine still yields an enzyme that exhibits some catalytic activity.[6] However, in this work these structures are not employed for modeling purposes, as we focus on the closed conformation; it is not clear whether the closed conformation is a prerequisite for enzyme activity.[6] On the other hand, the crystal structure of I14G DHFR was crystallized in the $P2_12_12$ space group, where both the M20 loop and the F-G loop (in direct contact with M20 loop) are partially disordered. This suggests that greater flexibility in the M20 loop may be observed in simulations of the I14G mutant.

dx.doi.org/10.1021/jp5059963 | J. Phys. Chem. B 2015, 119, 906−916

Comparison of the X-ray structures of the WT and I14G DHFR (Figure 3) shows noticeable conformational differences

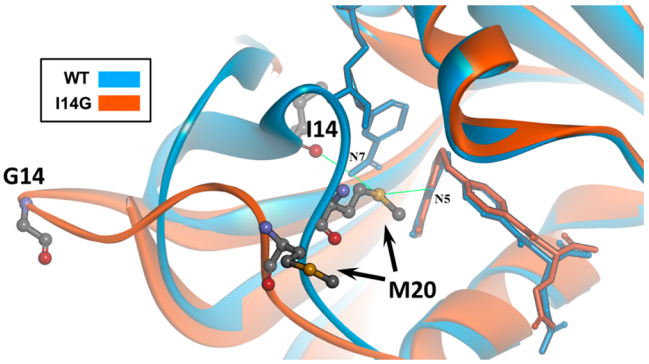

Figure 3. Superimposition of the X-ray crystal structures of the ternary complexes of WT (blue) and I14G (orange) DHFR. In the WT structure, both folate and $NADP^+$ ligands are bound (shown as sticks), whereas for I14G the nicotinamide-ribosyl moiety of $NADP^+$ is missing. The denoted amino acid residues (I14, G14, M20) are displayed as balls and sticks, with carbon, nitrogen, oxygen, and sulfur atoms colored gray, purple, red, and yellow, respectively. The interactions of the sulfur atom of the side chain of residue M20 in WT DHFR with the N5 position of the pterin ring (folate) and the N7 position of the nicotinamide ring ($NADP^+$) are marked with green lines, in addition to the hydrogen bond between N7 with the carbonyl oxygen of I14. In I14G DHFR, the M20 loop is located far from the ligands, incapable of making such contacts.

with regard to the M20 loop arrangement. In the WT enzyme, the side chain of residue M20 packs against the pterin ring of the substrate and is also close to the nicotinamide moiety of the cofactor. Consequently, the sulfur atom in the M20 side chain is within van der Waals contact distance with both the N5 atom of the pterin ring (3.68 Å) and the N7 position of the nicotinamide's carboxamide group (3.33 Å). This proximity allows the lone pair of the sulfur to maintain interactions with the bound ligands either via hydrogen bonding or through dative bonding, in addition to the hydrogen bonding between the N7 atom and the carbonyl oxygen of I14, which supports the nicotinamide ring in its binding site. Overall, this illuminates the possible role of the M20 residue as a mediator between the cofactor and the substrate, directing their relative position, thus facilitating the hydride transfer.[69] We also note that the M20 residue (and the M20 loop as a whole) adopts a very similar orientation in the complex of *ec*DHFR with the anticancer agent methotrexate (MTX) and NADPH (PDB ID 1RX3).[5] Conversely, in the crystal structure of the I14G mutant, the M20 loop is not well ordered, and the M20 side chain no longer points toward the ligands but is rather directed away from the active site. It seems that the M20 loop adopts a conformation unattainable in the WT DHFR, suggesting that I14G mutation might lead to enhanced flexibility of the loop. Assuming that the M20 loop is nonetheless partially closed during catalysis, we may ascribe the observed reduced rate of the hydride transfer in I14G DHFR relative to the WT enzyme[21] to a greater reorganization cost during the catalytic step. This slowing down corresponds to $\Delta\Delta G^{\ddagger}$ of ca. 4 kcal/mol.

It is instructive to see whether and how the proximal mutations affect the intrinsic structural characteristics of the species that are directly involved in the hydride transfer reaction. To this end, we followed several geometric variables during the course of the PMF simulations, including the antisymmetic stretch reaction coordinate, ζ_{asym}; the DAD, which was treated as a spectator coordinate (i.e., the spectator coordinate is *not* directly subject to a biasing force), denoted as ζ_{DAD}; and the donor−hydride−acceptor angle (∠D−H−A), all critical parameters of the reaction progress. Comparison of these properties at the TS is provided in Tables 1 and 2 at 25 °C (and at other temperatures in the Supporting Information, Tables S2 and S3). The slightly negative value of the antisymmetric stretch coordinate at the saddle point of the PMF, ($\zeta^{\ddagger}_{asym}$ ∼ −0.16 to −0.11 Å), suggests that the transition state is somewhat early, as can be seen from the PMF plots (Figure 2), and as expected from exothermic reactions (i.e., the Hammond Postulate).[22] This feature does not appear to be monotonically intensified or weakened with variation of the temperature in any of the DHFR systems, contrary to what has been observed previously.[68]

Table 1. Comparison of the CM and QM Transition State Positions for the Reaction in Wild-Type DHFR and I14 Mutants at 25 °C, in Terms of the Antisymmetric Stretch Coordinate, ζ_{asym}, and the Ensemble-Averaged Donor−Acceptor Distance (DAD) (Both in Å Units)

	$\zeta^{\ddagger}_{asym}$ [a]		$\langle\zeta_{DAD}\rangle^{\ddagger}_{\zeta asym}$ [d]	
	CM[b]	QM[c]	CM[b]	QM[c]
WT	−0.16	−0.18	2.65	2.67
	±0.01	±0.01	(0.06)	(0.05)
I14V	−0.13	−0.13	2.63	2.66
	±0.01	±0.01	(0.06)	(0.05)
I14A	−0.13	−0.13	2.64	2.66
	±0.01	±0.01	(0.06)	(0.05)
I14G	−0.11	−0.13	2.65	2.65
	±0.01	±0.01	(0.06)	(0.05)

[a]Determined from the saddle point of the classical mechanical PMF surface, obtained by combining the probability density statistics collected in the US simulations. [b]A bin size of 0.02 Å was used. [c]Nuclear quantum effects corrections for hydrogen were obtained from PI simulations, fitted to a cubic polynomial expression as a function of ζ_{asym}, and added to the CM-PMF. [d]Obtained by Boltzmann averaging of the DAD at $\zeta^{\ddagger}_{asym}$. Standard deviations are shown in parentheses.

The DAD in the GS (Table 2) is slightly elongated as a function of mutant perturbation (i.e., DAD(WT) ∼ DAD(I14V) < DAD(I14A) ∼ DAD(I14G)). The average DAD coordinate value obtained at the saddle point, $\zeta^{\ddagger}_{DAD}$, is 2.63−2.65 Å, *irrespective of the DHFR variants* and temperature. This distance is similar to that calculated previously for the transition state by other researchers. Using the EVB approach, Hammes-Schiffer and co-workers obtained transition state DAD values of 2.73[9]−2.74[10] Å, Miller and co-workers reported a value of 2.72 Å,[16] while Warshel and co-workers reported values in the range 2.6 to >3 Å.[14,70,71] Gao and co-workers obtained values ranging from 2.68[67] to 2.71[17] Å, using the QM(AM1)/MM Hamiltonian with a simple valence bond (SVB) correction. Interestingly, our results resemble the DAD in the optimized geometries of gas phase models, calculated at the AM1-SRP level (2.63 Å), and M06/6-31+G(d,p) and B3LYP-D/6-31+G(d,p) levels (2.66 Å).[22] This indicates that in the current simulations, the enzyme exerts a minor effect on the DAD. Furthermore, at these short DADs we expect only moderate

dx.doi.org/10.1021/jp5059963 | J. Phys. Chem. B 2015, 119, 906−916

Table 2. Ensemble-Averaged Structural Properties of WT DHFR and I14 Mutant at 25 °C at the Ground and Transition States[a]

	WT		I14V		I14A		I14G	
	GS	TS	GS	TS	GS	TS	GS	TS
C4N−H4N (Å)	1.11	1.29	1.11	1.31	1.11	1.31	1.11	1.31
	(0.03)	(0.03)	(0.03)	(0.03)	(0.03)	(0.03)	(0.03)	(0.03)
C6−H4N (Å)	2.98	1.40	2.95	1.38	3.05	1.41	3.04	1.40
	(0.04)	(0.03)	(0.03)	(0.03)	(0.03)	(0.03)	(0.03)	(0.03)
C4N−C6 (DAD) (Å)	3.96	2.65	3.94	2.63	4.07	2.64	4.06	2.65
	(0.09)	(0.06)	(0.10)	(0.06)	(0.08)	(0.06)	(0.09)	(0.06)
rehybridization (Å)	−1.2	−0.1	−1.1	0.0	−1.2	0.0	−1.2	−0.02
	(0.2)	(0.2)	(0.2)	(0.2)	(0.1)	(0.2)	(0.1)	(0.2)
C4N−H4N−C6 (∠D−H−A) (deg)	149	161	151	156	155	154	155	157
	(9)	(8)	(12)	(7)	(9)	(7)	(11)	(7)
N5−S(Met20) (Å)	3.8	4.1	4.3	3.9	4.0	3.7	4.3	4.2
	(0.3)	(0.5)	(0.4)	(0.3)	(0.6)	(0.5)	(0.4)	(0.6)
N7N−S(Met20) (Å)	3.8	3.7	4.1	3.8	4.2	4.2	4.1	4.2
	(0.3)	(0.4)	(0.4)	(0.3)	(0.3)	(0.4)	(0.5)	(0.4)
N7N−O(Ala7) (Å)	3.0	2.9	2.9	3.0	3.0	3.0	3.0	2.9
	(0.2)	(0.1)	(0.1)	(0.2)	(0.2)	(0.2)	(0.3)	(0.1)
N7N−O(Ile14) (Å)	3.1	3.3	3.0	3.1	3.1	3.1	3.1	3.0
	(0.2)	(0.3)	(0.2)	(0.2)	(0.2)	(0.2)	(0.3)	(0.2)
O7N−N(Ala7) (Å)	3.6	3.0	3.2	3.0	3.3	3.0	3.3	3.0
	(0.3)	(0.1)	(0.2)	(0.1)	(0.2)	(0.1)	(0.2)	(0.1)

[a]The properties were calculated from the structural data recorded during MD simulations, sorted into bins of ζ_{asym} with a width of 0.04 Å, and averaged over each bin. The values shown thus correspond to the ensemble of configurations falling within the bin associated with ζ_{GS} and $\zeta^{\ddagger}_{asym}$. Standard deviations per that bin are shown in parentheses.

tunneling effects, based on the fairly small NQE on the effective free energy barrier.

In addition, it should be noted that our findings agree with other recent computational studies, where the respective changes in the DAD at the reactant state (the Michaelis complex) and transition state of mutants of *ec*DHFR were found to be minor, if not negligible. For example, WT and G121V DHFR were predicted by Watney et al. to have an average DAD of 3.31 and 3.33 Å in the reactant state, respectively, while at the transition state, both systems were found to have an average DAD of 2.74 Å;[10] Likewise, Fan et al. computed an average DAD of 3.50 Å for the Michaelis complex in WT DHFR and 3.46 Å for the M42W/G121V double mutant, whereas these two had nearly identical average DAD at the transition state (2.71 and 2.70 Å, respectively).[17]

The invariability of the DAD at the TS in the mutant enzymes, relative to the WT, does not reflect the KIEs, their temperature dependence, or other components of a Marcus-like model. In the Marcus-like model the DAD is not simply the C−C distance of the reactive symmetric stretch coordinate at the saddle point of the PMF. Rather, in such phenomenological models, the relevant DADs constitute an ensemble of configurations, which are conducive to hydride transfer via a diffuse quantum mechanical state (i.e., tunneling ready state), which has nonzero contribution to the rate even at 3.0 Å.[21,66,72,73] Recently, we have shown that standard biased simulation methods might not be capable of capturing the fine details of transition state structures in enzymes.[26] Such slight differences do not have significant effects on the PMF, but could explain the substantial effects of the I14 mutants on the KIEs and their temperature dependence.

The donor−hydride−acceptor (D−H−A) angle is another useful geometric measure for tracking of the hydride ion position. The bending of the D−H−A angle at the transition state can quantify the extent to which the hydride transition path is bent relative to a hypothetical linear displacement along the axis connecting the DAD carbons. Generally speaking, in WT and I14V DHFR, this angle adopts an average of ca. 150° in the reactant state (Table 2). Fluctuations are observed toward the transition state during which the ∠D−H−A is widened by ∼5°, until it reaches a peak value. We note, though, that the maximum average ∠D−H−A is obtained slightly before or after, but not precisely at $\zeta^{\ddagger}_{asym}$, suggesting that the change in the D−H−A angle as the hydride transfers is not fully synchronized with the translation of the hydride. Pu et al. have observed this asynchronous nature of hydride transfer in DHFR previously.[74] As shown in Table 2, the average ∠D−H−A at $\zeta^{\ddagger}_{asym}$ is in the range 154−161° for both WT and mutant DHFRs. This result agrees well with that reported for the WT enzyme by Garcia-Viloca et al. (157°),[67] who employed a QM(AM1-SVB)/MM Hamiltonian. However, the angle is somewhat smaller compared to earlier computational studies of *ec*DHFR (162−166°)[9,75] and in vacuo calculations of model transition state structures (162°).[22] Much like our findings for the average DAD, the temperature hardly affects the variation of the average ∠D−H−A (Table S3).

The interactions between the pterin−nicotinamide complex with the enzyme matrix provide additional important structural information pertaining to the effect of the active-site mutations. In our simulations, the M20 loop is packed similarly against the reactive species in the GS and TS (Table 2 and S3). This contrasts the findings of Fan et al, where a slightly looser TS than GS was observed.[17] Furthermore, the hydrogen bonds between the nicotinamide moiety and backbone amide of A7 and I14 are kept largely intact in the simulations of WT and all mutants (Tables 2 and S3). However, in the GS, some of these hydrogen bonds are loosened, while at the TS, these hydrogen bonds are tightened.

We have also monitored various structural properties in the course of the extended QM/MM MD simulations of the

dx.doi.org/10.1021/jp5059963 | J. Phys. Chem. B 2015, 119, 906−916

Michaelis complex in the DHFR variants, covering dynamics within the active site and beyond. These include geometric changes within the reactants (such as the DAD), as well as hydrogen bonds between the bound ligands and surrounding protein residues. Figures 4 and 5 present selected time series

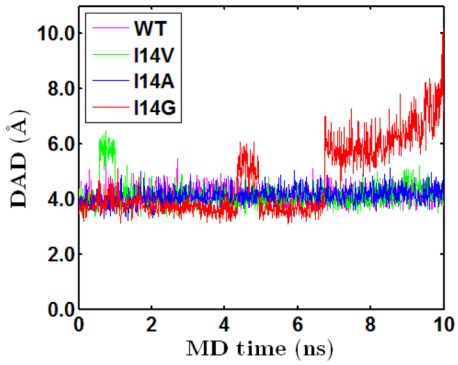

Figure 4. Time evolution series of the donor−acceptor distance during a 10 ns long MD trajectory of the Michaelis complex in WT and I14V, I14A, and I14G mutants of DHFR at 25 °C.

plots describing the evolution of WT and I14V, I14A, and I14G DHFR during MD at 25 °C. A validation set of time-series using an independent system setup is presented in Figure S8 and S9.

A rather striking difference between the GS dynamics of the WT and I14G ligand−protein complexes is demonstrated by the evolution of the DAD (Figure 4) and the hydrogen bonds involving the nicotinamide ring (Figure 5). In the WT enzyme, as well as in I14V and I14A, the DAD is rather stable, fluctuating around ca. 4.0 Å. However, in the I14G mutant, the DAD is subject to abrupt elongation, manifested by the movement of the nicotinamide−ribose moiety away from the pterin ring, in accordance with earlier MM MD simulations.[21] Analysis of the trajectories of the I14G complex reveals that the main changes in the NADPH geometry contributing to the increasing DAD often involve considerable rotation of the entire nicotinamide unit around the bond between the anomeric carbon of the ribose (the C1′ position) and the N1 position, as well as rotation of the amide group with respect to the dihydropyridine ring. As expected, these changes are accompanied by considerable weakening of the hydrogen bonds between the cofactor amide and the active-site residues 7 and 14. The M20 loop is slightly opened during this process, although a complete opening of the loop is not observed. In the case of I14V DHFR, we observe a rapid elongation and shortening of the DAD and the Ala7-NH---O-amide(NADPH) H-bond between ca. 0.5−1.0 ns of the MD simulations. In the second set of simulations of the Michaelis complex of the WT and I14 mutants (Figure S8 and S9), the same key active site interactions were monitored. In the case of the WT enzyme, these interactions remain intact throughout the 10 ns of the simulations. However, in all the I14 mutants, these interactions are lost as the nicotinamide moiety partially unbinds. Thus, our MD study of the Michaelis complex of WT DHFR shows that the closed conformation is stable for the duration of the simulations, while for the I14 mutants there is some unbinding of the nicotinamide−ribosyl moiety. In particular, the I14G mutant simulations show that the bound conformation is not stable. Nonetheless, the closed state is likely to be thermodynamically accessible during the hydride transfer step.

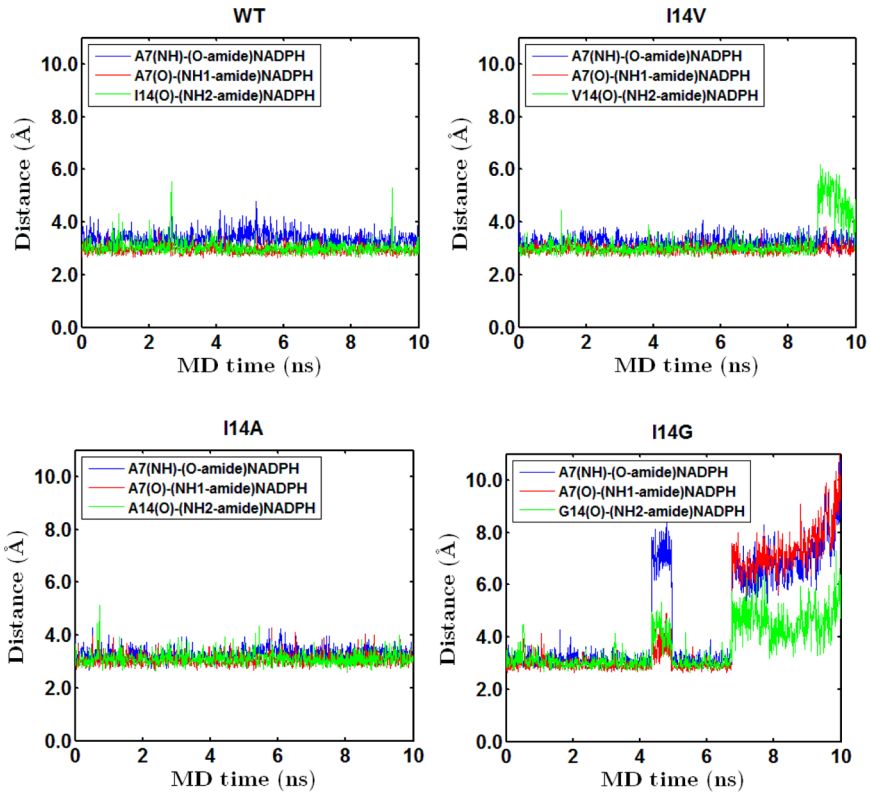

Figure 5. Time evolution series of selected hydrogen bonds during a 10 ns long MD trajectory of the Michaelis complex in WT and I14V, I14A, and I14G mutants of DHFR at 25 °C.

dx.doi.org/10.1021/jp5059963 | J. Phys. Chem. B 2015, 119, 906−916

4. DISCUSSION

The current multiscale MD simulation study investigated the hydride transfer in WT and I14 mutants of DHFR at several different temperatures relevant to our earlier experiments.[21] The simulations reproduce the effect of the active-site mutations on the free energy barrier height of the hydride transfer reaction in *ec*DHFR, in reasonable agreement with single-turnover rate measurements. The free energy simulations predict greater $\Delta G^{\ddagger}$'s for I14 mutants relative to the WT DHFR system. Furthermore, the increase in the free energy barriers are related to the extent of the side-chain perturbation, that is, $\Delta G^{\ddagger}(\mathrm{WT}) < \Delta G^{\ddagger}(\mathrm{I14V}) < \Delta G^{\ddagger}(\mathrm{I14A}) < \Delta G^{\ddagger}(\mathrm{I14G})$. The computed free energy barriers were also found to be rather insensitive to the temperatures investigated herein. Extended QM/MM MD simulations of the Michaelis complexes at ambient temperature show that the I14 mutants exhibit greater structural fluctuations than the WT enzyme, in accordance with our earlier MD simulations. This is particularly true for the GS DAD in I14G where the fluctuations are significant relative to those detected in the native enzyme. However, the TS configurations obtained from the current QM/MM MD simulations of the DHFR mutants exhibit similar active-site architecture to that seen in the TS ensemble of the WT enzyme, with very little variation in the average DADs. Changes in temperature were not found to modify these average DADs, and their influence is limited to minimal variations in the sampling distribution of the DADs at the TS. Based on the current simulations, the differences in activation free energy may be ascribed to a slight increase in the reorganization costs as the reaction proceeds from GS to TS in the mutant enzymes. We note that we initiated PMF simulations starting from systems equilibrated for 1, 5, and 10 ns. These simulations all gave similar DADs, PMFs and nuclear quantum effects.

From a computational perspective, one may ask whether the TS configurations generated by classical or quantum-corrected US simulations are representative of the hypothesized "tunneling ready state" (TRS) in the *ec*DHFR-catalyzed reaction. As noted above, in our multidimensional simulation approach, each distinct region in the phase space ("window") is sampled by restricting the antisymmetric stretch coordinate, ζ_{asym}, to certain positions, whereas no biasing forces are formally applied to the DAD coordinate. It is assumed that the DAD coordinate, ζ_{DAD}, independently adapts itself to the restrained configuration according to Boltzmann distribution, as other degrees of freedom do. In practice, the motion along the DAD cannot be completely separated from that associated with the C−H---C stretch, and therefore, the bias on ζ_{asym} inevitably affects the ζ_{DAD} as well, though indirectly. This partial coupling may be estimated by computing the Jacobian; however, this correction is expected to be small, as the D−H−A angle is nearly linear. Moreover, it is similar for the WT and different mutants at different temperatures. Another inherent assumption in the US technique is the complete relaxation of the enzyme-solvent environment along the reaction coordinate. This assumes a slow, progressive climbing of the reaction barrier. Furthermore, the motion along the reaction coordinate is not treated explicitly in such biased simulations, as the bias must be applied to allow barrier passing in a reasonable time. Thus, the barrier crossing motion itself is perturbed. This might explain the lack of temperature dependence we observe in the DAD, and the variation in the WT and mutant. These aspects warrant further studies.

Another computational aspect concerns sampling time and conformational effects, in particular the different conformational states associated with the M20 loop (Figure S7). As noted above, the initial configurations of both native and mutant Michaelis complexes of DHFR were modeled in this study (as in many other in silico investigations of *ec*DHFR) assuming that the M20 loop adopts a closed conformation during catalysis. In all four DHFR variants studied, the M20 loop remained in the closed, or partially closed, conformation throughout the US MD simulations. On the other hand, the crystal structure of I14G DHFR reported herein, where large parts of the M20 and F-G loops are poorly ordered, the position of M20 residue suggests that M20 loop faces away from the ligands, resulting in fewer stabilizing interactions with the reacting fragments (Figure 3). Although the prolonged MD equilibration of the Michaelis complex indicated intensified structural fluctuations in the I14G mutant relative to the WT enzyme (Figures 4 and 5), we did not observe a complete opening of the M20 loop that can be attributed to conformational exchange. The limited conformational space sampled by the DHFR variants is also manifested in the fact that the RMSD values of the M20 loop residues with respect to the starting coordinates did not exceed 1.5 Å.

The conformational stability of the Michaelis complex suggested by our simulations does not contradict available NMR data, given that NMR dispersion experiments for the WT enzyme observed conformational transitions (e.g., between closed to occluded states) only on the millisecond time-scale;[76,77] however, the current QM/MM MD simulations are restricted to the multiple-nanosecond time-scale and thus may not be able capture such large-scale processes. Indeed, Brooks and co-workers employed enhanced sampling simulations in order to elucidate the conformational transition pathway and the corresponding free energy profile in *ec*DHFR.[78] Their calculations showed that when the nicotinamide cofactor is in its binding pocket, the closed state of the enzyme is the most thermodynamically favorable conformation. However, because the free energy barriers separating the different states of the M20 loop are small (≤5 kcal/mol), the loop can practically populate multiple alternate conformations by thermal fluctuations at all times. In their studies, the flexibility of the M20 loop was quantified by measuring the C_α RMSD of the M20 loop relative to the reference crystallographic coordinates of the closed and occluded complexes. In particular, they found that the closed conformational ensemble contains two substates, including the "tightly-closed" conformation (RMSD 0.25−1.0 Å), in which the interactions of the cofactor and the substrate with the M20 side chain are enhanced, and the nicotinamide and pterin rings are oriented in an approximately coplanar fashion, as well as the more abundant "partially closed/open" conformation (RMSD 1.5−3.5 Å), where these two rings orient themselves approximately orthogonally to each other (see Figure 8 in ref 69). However, it was argued that it is only the former, minor substate that increases the pK_a of the N5 atom in dihydrofolate to a value as high as 6.5, thereby establishing appropriate conditions for a reaction to occur. Thus, the "tightly closed" conformation is considered as the catalytically active form.[69]

Moreover, using enhanced sampling simulations, the free energy profile along the entire conformational change pathway was delineated (see Scheme 3 in ref 78), which suggested that the transition between the closed and occluded states occurs through an intermediate "open" conformation.[78] The structural

dx.doi.org/10.1021/jp5059963 | J. Phys. Chem. B 2015, 119, 906−916

characteristics of the "tightly closed" complex described in the work of Brooks and co-workers are comparable to those observed in our own simulations of the Michaelis complex, although the mutant GS displayed some "partially closed/open" characteristics. Assuming that these two substates coexist in equilibrium, it will be essential to properly sample both states, and this will have implications on the evaluation of equilibrium properties obtained by ensemble averaging, such as partition functions. It might thus be important to consider multiple conformations of the Michaelis complex, each having its own reactivity, to account for experimentally observed enzyme kinetics. We also note that earlier studies of Brooks and co-workers have shown that distal mutations of *ec*DHFR alter the relative energy among the different M20 loop conformations, with respect to the WT enzyme.[11] In closing, we note that recent high-resolution crystal structures of *ec*DHFR at cryogenic and room temperatures have highlighted that cryo-cooling of crystals can perturb the energy landscape in DHFR.[79]

5. CONCLUSIONS

In summary, we have applied a hybrid quantum-classical methodology that can shed light on the interplay between enzyme kinetics, active-site architecture, structural dynamics, and nuclear quantum effects. Our strategy combines QM(AM1-SRP)/MM MD simulations with a PI-US approach to account for these aspects in catalysis of the hydride transfer reaction by WT *ec*DHFR and three I14 mutants. The free energy profiles computed in this work are in good agreement with available experimental single-turnover rate data obtained at a single temperature (25 °C). Structural analysis indicates that the Michaelis complex configuration is sensitive to I14 mutations, whereas the TSs obtained with US are rather insensitive both to the I14 mutations and temperature. Further studies are needed to elucidate other experimental findings such as KIEs and their temperature dependence.

■ ASSOCIATED CONTENT

Supporting Information

Classical and quantum free-energy surfaces (near the TS); CM and QM DAD distributions (at the TS); data tables with the free energies of activation and reaction and the KIEs for WT and I14V, I14A, and I14G DHFR at various temperatures; detailed comparison of geometric properties in the GS and TS of the four DHFR variants at 5, 25, and 45 °C; further discussion of X-ray diffraction findings is also provided. This material is available free of charge via the Internet at http://pubs.acs.org.

■ AUTHOR INFORMATION

Corresponding Author

*E-mail: majort@biu.ac.il.

Present Address

[#]Department of Cellular and Molecular Pharmacology, University of California, San Francisco, San Francisco, CA 94158, United States

Notes

The authors declare no competing financial interest.

■ ACKNOWLEDGMENTS

This work has been supported by the Israel Science Foundation and the United States-Israel Binational Science Foundation (Grant # 2012340). The work was also supported by the CyTera Project (NEA ΥΠΟΔΟΜΗ/ΣΤΡΑΤΗ/0308/31), which is cofunded by the European Regional Development Fund and the Republic of Cyprus through the Research Promotion Foundation. We thank Dr. Jay Nix at beamline 4.2.2 at the Advanced Light Source, Lawrence Berkeley National Laboratory for assistance with remote diffraction data collection. We thank the organizers and scientists at the workshop "CCP4 school: From data collection to structure refinement and beyond - June 2013" for assistance with data processing and refinement of the I14G DHFR mutant.

■ REFERENCES

(1) Hitchings, G. H.; Burchall, J. J. Inhibition of Folate Biosynthesis and Function as a Basis for Chemotherapy. *Adv. Enzymol. Relat. Areas Mol. Biol.* **1965**, 417−468.

(2) Huennekens, F. In Search of Dihydrofolate Reductase. *Protein Sci.* **1996**, *5*, 1201.

(3) Charlton, P.; Young, D.; Birdsall, B.; Feeney, J.; Roberts, G. Stereochemistry of Reduction of Folic Acid Using Dihydrofolate Reductase. *J. Chem. Soc., Chem. Commun.* **1979**, 922−924.

(4) Frey, P. A.; Hegeman, A. D. *Enzymatic Reaction Mechanisms*; Oxford University Press: New York, 2007.

(5) Sawaya, M. R.; Kraut, J. Loop and Subdomain Movements in the Mechanism of *Escherichia coli* Dihydrofolate Reductase: Crystallographic Evidence. *Biochemistry* **1997**, *36*, 586−603.

(6) Li, L.; C.J, F.; Wright, P. E.; Benkovic, S. J. Functional Role of a Mobile Loop of *Escherichia coli* Dihydrofolate Reductase in Transition-State Stabilization. *Biochemistry* **1992**, *31*, 7826−7833.

(7) Quaytman, S. L.; Schwartz, S. D. Reaction Coordinate of an Enzymatic Reaction Revealed by Transition Path Sampling. *Proc. Natl. Acad. Sci. U.S.A.* **2007**, *104*, 12253−12258.

(8) Dametto, M.; Antoniou, D.; Schwartz, S. D. Barrier Crossing in Dihydrofolate Reductase Does Not Involve a Rate-Promoting Vibration. *Mol. Phys.* **2012**, *110*, 531−536.

(9) Agarwal, P. K.; Billeter, S. R.; Hammes-Schiffer, S. Nuclear Quantum Effects and Enzyme Dynamics in Dihydrofolate Reductase Catalysis. *J. Phys. Chem. B* **2002**, *106*, 3283−3293.

(10) Watney, J. B.; Agarwal, P. K.; Hammes-Schiffer, S. Effect of Mutation on Enzyme Motion in Dihydrofolate Reductase. *J. Am. Chem. Soc.* **2003**, *125*, 3745−3750.

(11) Rod, T. H.; Radkiewicz, J. L.; Brooks, C. L., III Correlated Motion and the Effect of Distal Mutations in Dihydrofolate Reductase. *Proc. Natl. Acad. Sci. U.S.A.* **2003**, *100*, 6980−6985.

(12) Thorpe, I. F.; Brooks, C. L., III Barriers to Hydride Transfer in Wild Type and Mutant Dihydrofolate Reductase from *E. coli*. *J. Phys. Chem. B* **2003**, *107*, 14042−14051.

(13) Sergi, A.; Watney, J. B.; Wong, K. F.; Hammes-Schiffer, S. Freezing a Single Distal Motion in Dihydrofolate Reductase. *J. Phys. Chem. B* **2006**, *110*, 2435−2441.

(14) Liu, H.; Warshel, A. Origin of the Temperature Dependence of Isotope Effects in Enzymatic Reactions: The Case of Dihydrofolate Reductase. *J. Phys. Chem. B* **2007**, *111*, 7852−7861.

(15) Adamczyk, A. J.; Cao, J.; Kamerlin, S. C. L.; Warshel, A. Catalysis by Dihydrofolate Reductase and Other Enzymes Arises from Electrostatic Preorganization, Not Conformational Motions. *Proc. Natl. Acad. Sci. U.S.A.* **2011**, *108*, 14115−14120.

(16) Boekelheide, N.; Salomón-Ferrer, R.; Miller, T. F. Dynamics and Dissipation in Enzyme Catalysis. *Proc. Natl. Acad. Sci. U.S.A.* **2011**, *108*, 16159−16163.

(17) Fan, Y.; Cembran, A.; Ma, S.; Gao, J. Connecting Protein Conformational Dynamics with Catalytic Function as Illustrated in Dihydrofolate Reductase. *Biochemistry* **2013**, *52*, 2036−2049.

(18) Ruiz-Pernia, J. J.; Luk, L. Y. P.; García-Meseguer, R.; Martí, S.; Loveridge, E. J.; Tuñón, I.; Moliner, V.; Allemann, R. K. Increased Dynamic Effects in a Catalytically Compromised Variant of *Escherichia coli* Dihydrofolate Reductase. *J. Am. Chem. Soc.* **2013**, *135*, 18689−18696.

(19) Luk, L. Y. P.; Ruiz-Pernía, J. J.; Dawson, W. M.; Roca, M.; Loveridge, E. J.; Glowacki, D. R.; Harvey, J. N.; Mulholland, A. J.; Tuñón, I.; Moliner, V.; et al. Unraveling the Role of Protein Dynamics in Dihydrofolate Reductase Catalysis. *Proc. Natl. Acad. Sci. U.S.A.* **2013**, *110*, 16344−16349.
(20) Stojković, V.; Perissinotti, L. L.; Lee, J.; Benkovic, S. J.; Kohen, A. The Effect of Active-Site Isoleucine to Alanine Mutation on the DHFR Catalyzed Hydride-Transfer. *Chem. Commun.* **2010**, *46*, 8974−8976.
(21) Stojković, V.; Perissinotti, L. L.; Willmer, D.; Benkovic, S. J.; Kohen, A. Effects of the Donor−Acceptor Distance and Dynamics on Hydride Tunneling in the Dihydrofolate Reductase Catalyzed Reaction. *J. Am. Chem. Soc.* **2012**, *134*, 1738−1745.
(22) Doron, D.; Major, D. T.; Kohen, A.; Thiel, W.; Wu, X. Hybrid Quantum and Classical Simulations of the Dihydrofolate Reductase Catalyzed Hydride Transfer Reaction on an Accurate Semi-Empirical Potential Energy Surface. *J. Chem. Theory Comput.* **2011**, *7*, 3420−3437.
(23) Doron, D.; Kohen, A.; Major, D. T. Collective Reaction Coordinate for Hybrid Quantum and Molecular Mechanics Simulations: A Case Study of the Hydride Transfer in Dihydrofolate Reductase. *J. Chem. Theory Comput.* **2012**, *8*, 2484−2496.
(24) Engel, H.; Doron, D.; Kohen, A.; Major, D. T. Momentum Distribution as a Fingerprint of Quantum Delocalization in Enzymatic Reactions: Open-Chain Path-Integral Simulations of Model Systems and the Hydride Transfer in Dihydrofolate Reductase. *J. Chem. Theory Comput.* **2012**, *8*, 1223−1234.
(25) Roston, D.; Kohen, A.; Doron, D.; Major, D. T. Simulations of Remote Mutants of Dihydrofolate Reductase Reveal the Nature of a Network of Residues Coupled to Hydride Transfer. *J. Comput. Chem.* **2014**, *35*, 1411−1417.
(26) Doron, D.; Kohen, A.; Nam, K.; Major, D. T. How Accurate Are Transition States from Simulations of Enzymatic Reactions? *J. Chem. Theory Comput.* **2014**, *10*, 1863−1871.
(27) Vardi-Kilshtain, A.; Major, D. T.; Kohen, A.; Engel, H.; Doron, D. Hybrid Quantum and Classical Simulations of the Formate Dehydrogenase Catalyzed Hydride Transfer Reaction on an Accurate Semiempirical Potential Energy Surface. *J. Chem. Theory Comput.* **2012**, *8*, 4786−4796.
(28) Hwang, J. K.; Chu, Z. T.; Yadav, A.; Warshel, A. Simulations of Quantum Mechanical Corrections for Rate Constants of Hydride-Transfer Reactions in Enzymes and Solutions. *J. Phys. Chem.* **1991**, *95*, 8445−8448.
(29) Hwang, J. K.; Warshel, A. A Quantized Classical Path Approach for Calculations of Quantum Mechanical Rate Constants. *J. Phys. Chem.* **1993**, *97*, 10053−10058.
(30) Major, D. T.; Gao, J. L. Implementation of the Bisection Sampling Method in Path Integral Simulations. *J. Mol. Graph. Model.* **2005**, *24*, 121−127.
(31) Major, D. T.; Garcia-Viloca, M.; Gao, J. L. Path Integral Simulations of Proton Transfer Reactions in Aqueous Solution Using Combined QM/MM Potentials. *J. Chem. Theory Comput.* **2006**, *2*, 236−245.
(32) Major, D. T.; Gao, J. L. An Integrated Path Integral and Free-Energy Perturbation-Umbrella Sampling Method for Computing Kinetic Isotope Effects of Chemical Reactions in Solution and in Enzymes. *J. Chem. Theory Comput.* **2007**, *3*, 949−960.
(33) Jorgensen, W. L.; Chandrasekhar, J.; Madura, J. D.; Impey, R. W.; Klein, M. L. Comparison of Simple Potential Functions for Simulating Liquid Water. *J. Chem. Phys.* **1983**, *79*, 926−935.
(34) Jorgensen, W. L.; Maxwell, D. S.; Tirado-Rives, J. Development and Testing of the Opls All-Atom Force Field on Conformational Energetics and Properties of Organic Liquids. *J. Am. Chem. Soc.* **1996**, *118*, 11225−11236.
(35) Jorgensen, W. L.; Tirado-Rives, J. Molecular Modeling of Organic and Biomolecular Systems Using BOSS and MCPRO. *J. Comput. Chem.* **2005**, *26*, 1689−700.
(36) Warshel, A.; Levitt, M. Theoretical Studies of Enzymic Reactions: Dielectric, Electrostatic and Steric Stabilization of the Carbonium Ion in the Reaction of Lysozyme. *J. Mol. Biol.* **1976**, *103*, 227−249.
(37) Dewar, M. J. S.; Zoebisch, E. G.; Healy, E. F.; Stewart, J. J. P. AM1: A New General Purpose Quantum Mechanical Molecular Model. *J. Am. Chem. Soc.* **1985**, *107*, 3902−3909.
(38) Rossi, I.; Truhlar, D. G. Parameterization of NDDO Wavefunctions Using Genetic Algorithms. An Evolutionary Approach to Parameterizing Potential Energy Surfaces and Direct Dynamics Calculations for Organic Reactions. *Chem. Phys. Lett.* **1995**, *233*, 231−236.
(39) MacKerell, A. D., Jr.; Bashford, D.; Bellott; Dunbrack, R. L.; Evanseck, J. D.; Field, M. J.; Fischer, S.; Gao, J.; Guo, H.; Ha, S.; et al. All-Atom Empirical Potential for Molecular Modeling and Dynamics Studies of Proteins. *J. Phys. Chem. B* **1998**, *102*, 3586−3616.
(40) MacKerell, A. D., Jr.; Feig, M.; Brooks, C. L., III Extending the Treatment of Backbone Energetics in Protein Force Fields: Limitations of Gas-Phase Quantum Mechanics in Reproducing Protein Conformational Distributions in Molecular Dynamics Simulations. *J. Comput. Chem.* **2004**, *25*, 1400−1415.
(41) Best, R. B.; Zhu, X.; Shim, J.; Lopes, P. E. M.; Mittal, J.; Feig, M.; MacKerell, A. D., Jr. Optimization of the Additive CHARMM All-Atom Protein Force Field Targeting Improved Sampling of the Backbone ϕ, ψ and Side-Chain χ_1 and χ_2 Dihedral Angles. *J. Chem. Theory Comput.* **2012**, *8*, 3257−3273.
(42) Best, R. B.; Mittal, J.; Feig, M.; MacKerell, A. D., Jr. Inclusion of Many-Body Effects in the Additive CHARMM Protein CMAP Potential Results in Enhanced Cooperativity of α-Helix and β-Hairpin Formation. *Biophys. J.* **2012**, *103*, 1045−1051.
(43) Dror, R. O.; Dirks, R. M.; Grossman, J.; Xu, H.; Shaw, D. E. Biomolecular Simulation: A Computational Microscope for Molecular Biology. *Annu. Rev. Biophys.* **2012**, *41*, 429−452.
(44) Nam, K.; Gao, J.; York, D. M. An Efficient Linear-Scaling Ewald Method for Long-Range Electrostatic Interactions in Combined QM/MM Calculations. *J. Chem. Theory Comput.* **2004**, *1*, 2−13.
(45) Andersen, H. C. Molecular Dynamics Simulations at Constant Pressure and/or Temperature. *J. Chem. Phys.* **1980**, *72*, 2384−2393.
(46) Hoover, W. G. Canonical Dynamics: Equilibrium Phase-Space Distributions. *Phys. Rev. A* **1985**, *31*, 1695−1697.
(47) Hockney, R. W. The Potential Calculation and Some Applications. *Meth. Comput. Phys.* **1970**, *9*, 135−211.
(48) Ryckaert, J.-P.; Ciccotti, G.; Berendsen, H. J. C. Numerical Integration of the Cartesian Equations of Motion of a System with Constraints: Molecular Dynamics of *N*-Alkanes. *J. Comput. Phys.* **1977**, *23*, 327−341.
(49) Brooks, B. R.; Bruccoleri, R. E.; Olafson, B. D.; States, D. J.; Swaminathan, S.; Karplus, M. CHARMM: A Program for Macromolecular Energy, Minimization, and Dynamics Calculations. *J. Comput. Chem.* **1983**, *4*, 187−217.
(50) Brooks, B. R.; Brooks, C. L., III; MacKerell, A. D., Jr.; Nilsson, L.; Petrella, R. J.; Roux, B.; Won, Y.; Archontis, G.; Bartels, C.; Boresch, S.; et al. CHARMM: The Biomolecular Simulation Program. *J. Comput. Chem.* **2009**, *30*, 1545−1614.
(51) Torrie, G. M.; Valleau, J. P. Nonphysical Sampling Distributions in Monte Carlo Free-Energy Estimation: Umbrella Sampling. *J. Comput. Phys.* **1977**, *23*, 187−199.
(52) Kumar, S.; Rosenberg, J. M.; Bouzida, D.; Swendsen, R. H.; Kollman, P. A. The Weighted Histogram Analysis Method for Free-Energy Calculations on Biomolecules. I. The Method. *J. Comput. Chem.* **1992**, *13*, 1011−1021.
(53) Cameron, C. E.; Benkovic, S. J. Evidence for a Functional Role of the Dynamics of Glycine-121 of *Escherichia coli* Dihydrofolate Reductase Obtained from Kinetic Analysis of a Site-Directed Mutant. *Biochemistry* **1997**, *36*, 15792−15800.
(54) Kabsch, W. Xds. *Acta. Cryst. D* **2010**, *66*, 125−132.
(55) Pflugrath, J. W. The Finer Things in X-Ray Diffrcation Data Collection. *Acta. Cryst. D* **1999**, *55*, 1718−1725.
(56) McCoy, A. J.; Grosse-Kunstleve, R. W.; Adama, P. D.; Winn, M. D.; Storoni, L. C.; Read, R. J. *Phaser* Crystallographic Software. *J. Appl. Crystallogr.* **2007**, *40*, 658−674.

(57) Collaborative Computational Project, N., The *CCP4* Suite: Programs for Protein Crystallography. *Acta. Cryst. D* **1994**, *50*, 760−763.
(58) Murshundov, G. N.; Vagin, A. A.; Dodson, E. J. Refinement of Macromolecular Structures by the Maximum-Likelihood Method. *Acta. Cryst. D* **1997**, *53*, 240−255.
(59) Emsley, P.; Cowtan, K. *Coot*: Model-Building Tools for Molecular Graphics. *Acta. Cryst. D* **2004**, *60*, 2126−2132.
(60) Rajagopalan, P. T. R.; Lutz, S.; Benkovic, S. J. Coupling Interactions of Distal Residues Enhance Dihydrofolate Reductase Catalysis: Mutational Effects on Hydride Transfer Rates. *Biochemistry* **2002**, *41*, 12618−12628.
(61) Swanwick, R. S.; Maglia, G.; Tey, L.-h.; Allemann, R. K. Coupling of Protein Motions and Hydrogen Transfer During Catalysis by *Escherichia coli* Dihydrofolate Reductase. *Biochem. J.* **2006**, *394*, 259−265.
(62) Loveridge, E. J.; Allemann, R. K. Effect of pH on Hydride Transfer by *Escherichia coli* Dihydrofolate Reductase. *ChemBioChem* **2011**, *12*, 1258−1262.
(63) Sikorski, R. S.; Wang, L.; Markham, K. A.; Rajagopalan, P. T. R.; Benkovic, S. J.; Kohen, A. Tunneling and Coupled Motion in the *Escherichia coli* Dihydrofolate Reductase Catalysis. *J. Am. Chem. Soc.* **2004**, *126*, 4778−4779.
(64) Fierke, C. A.; Johnson, K. A.; Benkovic, S. J. Construction and Evaluation of the Kinetic Scheme Associated with Dihydrofolate Reductase from *Escherichia coli*. *Biochemistry* **1987**, *26*, 4085−4092.
(65) Loveridge, E. J.; Tey, L.-H.; Behiry, E. M.; Dawson, W. M.; Evans, R. M.; Whittaker, S. B. M.; Günther, U. L.; Williams, C.; Crump, M. P.; Allemann, R. K. The Role of Large-Scale Motions in Catalysis by Dihydrofolate Reductase. *J. Am. Chem. Soc.* **2011**, *133*, 20561−20570.
(66) Wang, L.; Goodey, N. M.; Benkovic, S. J.; Kohen, A. Coordinated Effects of Distal Mutations on Environmentally Coupled Tunneling in Dihydrofolate Reductase. *Proc. Natl. Acad. Sci. U.S.A.* **2006**, *103*, 15753−15758.
(67) Garcia-Viloca, M.; Truhlar, D. G.; Gao, J. Reaction-Path Energetics and Kinetics of the Hydride Transfer Reaction Catalyzed by Dihydrofolate Reductase. *Biochemistry* **2003**, *42*, 13558−13575.
(68) Pu, J.; Ma, S.; Gao, J.; Truhlar, D. G. Small Temperature Dependence of the Kinetic Isotope Effect for the Hydride Transfer Reaction Catalyzed by *Escherichia coli* Dihydrofolate Reductase. *J. Phys. Chem. B* **2005**, *109*, 8551−8556.
(69) Khavrutskii, I.; Price, D.; Lee, J.; Brooks, C. L., III Conformational Change of the Methionine 20 Loop of *Escherichia coli* Dihydrofolate Reductase Modulates pK_a of the Bound Dihydrofolate. *Protein Sci.* **2007**, *16*, 1087.
(70) Liu, H.; Warshel, A. The Catalytic Effect of Dihydrofolate Reductase and Its Mutants Is Determined by Reorganization Energies. *Biochemistry* **2007**, *46*, 6011−6025.
(71) Roca, M.; Liu, H.; Messer, B.; Warshel, A. On the Relationship between Thermal Stability and Catalytic Power of Enzymes. *Biochemistry* **2007**, *46*, 15076−15088.
(72) Roston, D.; Cheatum, C. M.; Kohen, A. Hydrogen Donor-Acceptor Fluctuations from Kinetic Isotope Effects: A Phenomenological Model. *Biochemistry* **2012**, *51*, 6860−6870.
(73) Klinman, J. P.; Kohen, A. Hydrogen Tunneling Links Protein Dynamics to Enzyme Catalysis. *Annu. Rev. Biochem.* **2013**, *82*, 471−496.
(74) Pu, J.; Ma, S.; Garcia-Viloca, M.; Gao, J.; Truhlar, D. G.; Kohen, A. Nonperfect Synchronization of Reaction Center Rehybridization in the Transition State of the Hydride Transfer Catalyzed by Dihydrofolate Reductase. *J. Am. Chem. Soc.* **2005**, *127*, 14879−14886.
(75) Castillo, R.; Andrés, J.; Moliner, V. Catalytic Mechanism of Dihydrofolate Reductase Enzyme. A Combined Quantum-Mechanical/Molecular-Mechanical Characterization of Transition State Structure for the Hydride Transfer Step. *J. Am. Chem. Soc.* **1999**, *121*, 12140−12147.
(76) McElheny, D.; Schnell, J. R.; Lansing, J. C.; Dyson, H. J.; Wright, P. E. Defining the Role of Active-Site Loop Fluctuations in Dihydrofolate Reductase Catalysis. *Proc. Natl. Acad. Sci. U.S.A.* **2005**, *102*, 5032−5037.
(77) Boehr, D. D.; McElheny, D.; Dyson, H. J.; Wright, P. E. The Dynamic Energy Landscape of Dihydrofolate Reductase Catalysis. *Science* **2006**, *313*, 1638−1642.
(78) Arora, K.; Brooks, C. L., III Functionally Important Conformations of the Met20 Loop in Dihydrofolate Reductase Are Populated by Rapid Thermal Fluctuations. *J. Am. Chem. Soc.* **2009**, *131*, 5642−5647.
(79) Keedy, D. A.; van den Bedem, H.; Sivak, D. A.; Petsko, G. A.; Ringe, D.; Wilson, M. A.; Fraser, J. S. Crystal Cryocooling Distorts Conformational Heterogeneity in a Model Michaelis Complex of DHFR. *Structure* **2014**, *22*, 899−910.